

# Solid-state synthesis of monocrystalline iron oxide nanoparticle based ferrofluid suitable for magnetic resonance imaging contrast application

Jun Lu<sup>1</sup>, Shihe Yang<sup>2,6</sup>, Ka Ming Ng<sup>1</sup>, Chia-Hao Su<sup>3,4</sup>,  
Chen-Sheng Yeh<sup>3</sup>, Ya-Na Wu<sup>5</sup> and Dar-Bin Shieh<sup>5</sup>

<sup>1</sup> Department of Chemical Engineering, The Hong Kong University of Science and Technology, Clear Water Bay, Kowloon, Hong Kong

<sup>2</sup> Department of Chemistry, The Hong Kong University of Science and Technology, Clear Water Bay, Kowloon, Hong Kong

<sup>3</sup> Department of Chemistry and Center for Micro/Nano Science and Technology, National Cheng Kung University, Tainan 701, Taiwan

<sup>4</sup> Interdisciplinary MRI/MRS Lab, Department of Electrical Engineering, National Taiwan University, Taipei 106, Taiwan

<sup>5</sup> Institute of Oral medicine and Center for Micro/Nano Science and Technology, National Cheng Kung University College of Medicine, Tainan 701, Taiwan

E-mail: [chsyang@ust.hk](mailto:chsyang@ust.hk)

Received 14 August 2006, in final form 11 October 2006

Published 16 November 2006

Online at [stacks.iop.org/Nano/17/5812](http://stacks.iop.org/Nano/17/5812)

## Abstract

A new  $\gamma$ -Fe<sub>2</sub>O<sub>3</sub> MION ferrofluid has been developed with a salt-assisted solid-state reaction. Characterizations show that the ferrofluid is composed of maghemite nanoparticles with a mean diameter of 2.7 nm. Though the nanoparticles are ultrafine, they are well crystallized, with a saturation magnetization value of 34.7 emu g<sup>-1</sup>, making them suitable for MRI applications. In spite of the absence of any surfactant, the ferrofluid can be stable for more than 6 months. An *in vitro* cytotoxicity test revealed good biocompatibility of the maghemite nanoparticles, suggesting that they may be further explored for biomedical applications. NMR measurements revealed significantly reduced water proton relaxation times  $T_1$  and  $T_2$ . The MR images of the nanoparticles in aqueous dispersion were investigated using a 3 T clinical MR imager. These preliminary experiments have demonstrated the potential of the as-synthesized ultrafine, cap-free maghemite MIONs in functional molecular imaging for biomedical research and clinical diagnosis.

(Some figures in this article are in colour only in the electronic version)

 Supplementary data files are available from [stacks.iop.org/Nano/17/5812](http://stacks.iop.org/Nano/17/5812)

## 1. Introduction

Magnetite and maghemite nanoparticles are of considerable interest because of their unique characteristics, such as superparamagnetism, high saturation fields, and extra anisotropy contributions, which arise from the effects of finite size and

large surface area [1]. Such characteristics allow the pragmatic and potential applications of the magnetic nanoparticles to sprawl into many areas of biotechnology. The magnetic nanoparticles are especially useful in biomedicine when they are dispersed into water to form ferrofluids, which can be used, for example, as image contrast agents in magnetic resonance imaging (MRI) [2–6], vehicles for drug delivery [7], and antennae for hyperthermia [8–10].

<sup>6</sup> Author to whom any correspondence should be addressed.

Superparamagnetic iron oxide (SPIO) nanoparticles have been extensively studied over the past decade for MR  $T_1$  and  $T_2/T_2^*$  relaxation contrast agents (CAs) [2–6]. Monocrystalline iron oxide nanoparticles (MIONs) are a kind of SPIO nanoparticle that have the smallest particle size (<10 nm), such as the commercially available SPIOs with a monocrystalline core of 4–6 nm and a dextran coating. Large SPIO nanoparticles (>40 nm) are efficiently accumulated in reticuloendothelial systems (about 80% of the injected dose in liver and 5–10% in the spleen) and have a plasma half-life shorter than 10 min [11]. MIONs, however, are not immediately recognized by the reticuloendothelial systems thanks to their ultrasmall size with a consequent plasma half-life longer than 2 h [6, 12]. Therefore, they can remain in the blood long enough to act as blood-pool agents for MR angiography (MRA). Besides, the ultrasmall size allows MIONs to easily pass through capillary endothelium while retaining superparamagnetism [2, 13, 14]. These features make MIONs ideal CAs for MRI probing of receptor-directed and magnetically labelled cells.

Initial MRI studies used gadolinium chelates as a receptor-directed agent, but very high levels of this CA were needed to significantly reduce proton relaxation times, which are not ideally practicable. MIONs provide higher magnetic susceptibility (by two to three orders of magnitude) than gadolinium. It has been stated that *in vivo* MRI detection is possible at a concentration as low as 1  $\mu\text{g}$  Fe/g tissue. Targeted MRI with MIONs is still in the experimental stage, but may prove to be a powerful tool for cellular and molecular investigations in the future [2, 6, 13, 14].

Due to their chemical/thermal stability and biocompatibility, maghemite nanoparticles are often the magnetic agents of choice in the biomedical field compared to magnetite nanoparticles. There are a number of ways to prepare maghemite nanoparticles, such as coprecipitation, microemulsions, high temperature decomposition of organic precursors and oxidation of magnetite nanoparticles [15–18]. However, the methods reported so far have the disadvantages of the need to use expensive organic precursors as starting materials, tedious washing procedures for surfactants, or particle aggregations during high temperature oxidation in the air. Besides, the particle sizes are usually larger than 10 nm. Therefore, the development of new, convenient and large-scale synthesis methods for maghemite nanoparticles, especially the MIONs, is still a major challenge.

Mechanochemical processing is a novel method to synthesize nanostructured materials. It is an organic-solvent-free process and thus ecologically clean. Besides, solid-state synthesis is particularly suitable for large-scale production because of its simplicity and low cost. Although synthesis of maghemite nanoparticles with an average diameter of 15 nm was reported by high energy ball-milling with iron powder and water [19], at least 48 h was needed for the milling process and the product was severely aggregated. Direct phase transformation from haematite to maghemite is possible by grinding in ethanol medium [20], but the product is normally a mixture of haematite and maghemite phases. Lin *et al* used anhydrous ferric and ferrous chlorides as reactants for the solid-state synthesis of magnetite nanoparticles with an average particle size of 14.8 nm, but again the method suffered from a long milling time (>72 h).

At present, all of the iron oxide nanoparticles already approved for clinical usage as MRI CAs, as well as most of the currently developing CAs, are stabilized by dextran or its derivatives [3, 22–24]. The polymer coating significantly increases their overall size and therefore may limit their tissue distribution, penetration, and metabolic clearance. Polymer-coated particles are often taken up rapidly by the reticuloendothelial system, such as Kupffer cells of the liver [3, 6, 25]. Cheng *et al* recently reported the synthesis of well dispersed  $\text{Fe}_3\text{O}_4$  nanoparticles protected by  $(\text{N}(\text{CH}_3)_4\text{OH})$  [3]. The surfaces of the nanoparticles were covered by hydroxyl groups incorporated with  $^+\text{N}(\text{CH}_3)_4$  via electrostatic interaction. Although the resulting magnetite particles exhibited excellent biocompatibility, the native surface chemistry of the methyl groups from  $^+\text{N}(\text{CH}_3)_4$  does not seem to permit further biochemical modifications of the nanoparticles easily.

In this paper, we report on the synthesis of maghemite nanoparticles with a mean diameter down to 2.7 nm by using a new mechanochemical method. Here ferric/ferrous hydrate chlorides were used as reactants instead of metallic iron powder, haematite powder, and anhydrous ferric/ferrous chlorides normally used for the synthesis of iron oxide nanoparticles [19–21]. With this method, a high yield can be achieved with a milling time as short as only 1 h. The MIONs we synthesized have a narrow particle size distribution and can be readily dispersed into ferrofluid for MRI application. The abundant surface hydroxyl groups render the nanoparticles highly water-soluble with no need for the addition of stabilizing surfactants. Moreover, this will allow for further biochemical modifications.

## 2. Experimental section

### 2.1. Preparation of maghemite nanoparticles

Iron (II) chloride tetrahydrate ( $\text{FeCl}_2 \cdot 4\text{H}_2\text{O}$ ) (99%), iron (III) chloride hexahydrate ( $\text{FeCl}_3 \cdot 6\text{H}_2\text{O}$ ) (99%) and potassium chloride (99.5%) were purchased from Aldrich. Potassium hydroxide (purum,  $\geq 85\%$ ) was obtained from Fluka.

For the synthesis of maghemite nanoparticles, mixed powders of 1.35 g  $\text{FeCl}_3 \cdot 6\text{H}_2\text{O}$  (0.005 mol), 0.50 g  $\text{FeCl}_2 \cdot 4\text{H}_2\text{O}$  (0.0025 mol) and 3.9 g KCl were ground in a mortar at room temperature for 30 min. The mixture obtained from grinding was a yellow paste. To the mortar was added KOH powder (0.02 mol, 1.22 g), followed by grinding for another 30 min at room temperature. During the KOH addition and the subsequent grinding, a significant amount of heat and some vapour was given off in the first few minutes. At the same time, the reactant mixture became dark brown and dry. Repeated sonication and washing with DDI (double deionized) water followed until no  $\text{Cl}^-$  ion could be detected. The sample was then centrifuged (Sorvall® RC26 plus; Sorvall Instruments, Dupont, Wilmington, DE) at 2000 rpm for 10 min. The nanoparticles were finally prepared in the form of either colloid or powder for characterizations. With the procedures described above, a dark brown transparent colloid was obtained with a loading of  $\gamma\text{-Fe}_2\text{O}_3$  nanoparticles as high as 6 mg (Fe)  $\text{ml}^{-1}$  (0.11 M Fe content). The pH value of the colloid was between 4 and 5. A gel electrophoresis

experiment showed that the colloid was negatively charged. To obtain a powder sample the colloid was filtered by a 0.1  $\mu\text{m}$  membrane. The precipitate was collected and vacuum dried at 50 °C for 6 h, and then cooled down to room temperature. The powder weighed 0.49 g, which corresponds to a yield of 81%.

## 2.2. Characterizations

Electron micrographs of the maghemite nanoparticles colloids were taken using a JEOL JEM 2010F, with capabilities of energy dispersive x-ray spectroscopy (EDXS) and selected area electron diffraction (SAED). The particle size and size distribution analyses were carried out by measuring diameters of 100 particles selected randomly from appropriate TEM images. For a particle with an irregular shape, a mean value of the diameter was given by taking account of both long and short dimensions of the nanoparticle. The TEM samples were prepared by dropping an aqueous dispersion of the nanoparticles onto a copper mesh coated with an amorphous carbon film, followed by drying in a vacuum desiccator. XRD data were collected on a Philips PW1830 powder x-ray diffractometer employing Cu K $\alpha$  radiation ( $\lambda = 1.54056 \text{ \AA}$ ) at 40 kV and 40 mA. Thermogravimetric analysis (TGA) and differential thermal analysis (DTA) were conducted in air on a Perkin Elmer UNIX/TGA7 thermal analyser at a heating rate of 10 °C min<sup>-1</sup> from room temperature to 800 °C or above. X-ray photoelectron spectroscopy (XPS) was performed using an Al K $\alpha$  source (14 kV and 350 W). The binding energy scale was calibrated to 285.0 eV for the main C (1s) peak. For FTIR measurements (Perkin Elmer, Spectrum One FT-IR spectrophotometer), the maghemite nanoparticle powders were ground together with KBr before measurement. Magnetization data were acquired on a LakeShore vibrating sample magnetometer (model 7037/9509-P VSM). The content of iron in the ferrofluid was determined by a Perkin Elmer Optima-3000XL ICP-AES.

## 2.3. *In vitro* cytotoxicity evaluation

For the evaluation of biocompatibility of the as-synthesized nanoparticles, Vero cells at a density of 5000 cells/well were cultured in 96-well plates containing minimum essential medium with 2 mM L-glutamine and Earle's BSS adjusted to contain 1.5 g l<sup>-1</sup> sodium bicarbonate, 0.1 mM non-essential amino acids, 1 mM sodium pyruvate and 10% foetal bovine serum (FBS). The cells were maintained at 37 °C with 5% CO<sub>2</sub> in the air. After 24 h of incubation, the culture medium was replaced with fresh culture medium or medium containing iron oxide nanoparticles in 100, 10, 1, 0.1, 0.01, and 0.001  $\mu\text{g ml}^{-1}$ , incubated for an additional 4 h, and washed twice with phosphate buffered saline (PBS). The cells were then given fresh culture medium and further incubated for 48 h. Afterwards, the medium was replaced with 100  $\mu\text{l}$  of fresh culture medium containing 10  $\mu\text{l}$  of WST-1 reagent (Roche Applied Science, USA) and incubated for an additional 2 h. The plate was briefly centrifuged and 90  $\mu\text{l}$  of the culture medium was transferred to an ELISA plate and subjected to the spectrophotometric quantification of cell viability by optical absorbance (450/690 nm) using an ELISA plate reader (Tecan, Mannedorf, Switzerland). The cell culture wells were then processed for Pearl's iron stain and counterstained

with Nuclear Fast Red. The cells were photographed with a CCD camera under light microscopy (Axiovert 135, Zeiss, Germany).

## 2.4. Haemocompatibility test

Fresh human blood was collected from a healthy donor and stored in a Vacutainer tube containing heparin as anticoagulant (BD Biosciences, CA, USA). Five microlitres of blood was placed in each tube, containing different concentrations of nanoparticles or the negative control of isotonic phosphate buffered solution (PBS) alone. For the positive control, the blood cells were lysed in 0.1% sodium carbonate solution. All the samples were incubated at 37 °C to imitate human body temperature for 1, 2 and 4 h. The blood cells were removed by centrifugation at 340  $\times g$  for 15 min followed by removal of nanoparticles at 20 000  $\times g$  for 30 min. The haemolysis index was measured by the presence of free haemoglobin with optical absorbance at 545 nm by a spectrophotometer. The positive control was set as 100% haemolysis, and the negative control as 0% haemolysis. A test result less than 5% was recognized as haemocompatible. The whole experiment was triplicated.

## 2.5. Characterization of $r_1$ and $r_2$ relaxivities and magnetic resonance imaging

The experiments were performed in a 3 T MRI Biospec system (Bruker Companies, Ettlingen, Germany). We used a high-performance gradient coil mounted on the table of the 3 T magnet, with an inner diameter = 6 cm and a maximal gradient strength = 1000 mT m<sup>-1</sup>, and a quadrature coil with inner diameter of 3.5 cm for RF transmission and reception. For *in vitro* MR imaging and  $T_1$ ,  $T_2$  measurements, all nanoparticles were dispersed in water at various concentrations (0, 10<sup>-1</sup>, 5  $\times$  10<sup>-2</sup>, 10<sup>-2</sup>, 5  $\times$  10<sup>-3</sup>, 10<sup>-3</sup>, 5  $\times$  10<sup>-4</sup>, 10<sup>-4</sup>, 10<sup>-5</sup>, 10<sup>-6</sup>, 10<sup>-7</sup>, 10<sup>-8</sup>, 10<sup>-9</sup>, 10<sup>-10</sup>, and 10<sup>-11</sup> M). The images were taken using the designed sequences in the matrix size of 256  $\times$  192 with the field of view being 60  $\times$  60 mm<sup>2</sup> and 6 mm slice thickness. The sequence parameters were as follows. (1) For the  $T_1$  weighted image: fast spin echo with repetition time (TR) = 472 ms; echo time (TE) = 9.4 ms; number of averages = 8. (2) For the  $T_2$  weighted sequence: fast spin echo with TR/TE = 4500 ms/65 ms, number of averages = 6. (3) For the  $T_2^*$  weighted image: gradient echo with TR/TE/flip angle = 600 ms/5 ms/30°; number of averages = 6.  $T_1$  measurements were performed using a standard spin-echo sequence (PVM-MSME) with a repetition time (TR) of 6000 ms, an echo time (TE) of 8.7 ms and 45 inversion recovery times (TI) (13.3–6000 ms). The field of view was 60 mm and the image plane was 128  $\times$  128 with 6 mm slice thickness; this allowed for simultaneous imaging of 26 vials containing 0.3 ml of different CA concentrations and nanomaterials, respectively. The signal containing on average 50 voxels was then evaluated for all TI values.  $T_2$  measurements were performed via a PVM-MSME pulsed sequence with (TR/TE) of 4000 ms/10.1 ms. The number of echoes collected was 60 and the number of averages was five. The field of view was 60  $\times$  60 mm<sup>2</sup> and the image plane was 256  $\times$  192 with 6 mm of slice thickness.

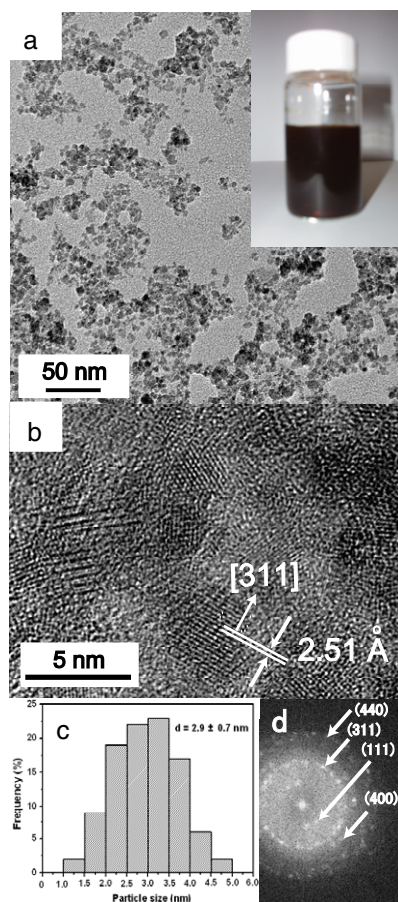


**Figure 1.** As-synthesized maghemite colloid nanoparticles dispersed in aqueous solution. (a) Large area TEM image; (b) high resolution TEM image; (c) size distribution histogram; (d) SAED pattern. The inset of (a) is a photograph of the ferrofluid containing 0.11 M [Fe]  $\gamma$ -Fe<sub>2</sub>O<sub>3</sub>.

### 3. Results and discussion

#### 3.1. Preparation and characterization of maghemite nanoparticles

Shown in figure 1 are the morphological and structural characteristics of the as-synthesized maghemite MION ferrofluid. It can be seen in the large area TEM images of figure 1(a) that the colloids are well dispersed and aggregation is minimal. The particles are almost spherical with ultrafine sizes. From the size distribution histogram of the ferrofluid sample shown in figure 1(c), we obtain an average particle size and standard deviation ( $\sigma$ ) of 2.9 and 0.7 nm, respectively. An individual nanoparticle with a diameter larger than 5 nm or smaller than 1 nm can hardly be found in all of the TEM images we acquired. Though the nanoparticles are ultrafine in size, they are all well crystallized as can be seen from the high resolution TEM image in figure 1(b). At the bottom of figure 1(b) is a spherical and well crystallized nanoparticle with a diameter of 4.7 nm. Regular fringes are clearly observed in the nanoparticle with a spacing of 2.51 Å, which is exactly the (311) interplanar distance of the tetragonal iron oxide, maghemite (2.51 Å in JCPDS file No 25-1402). The SAED pattern of the sample (figure 1(d)) exhibits four

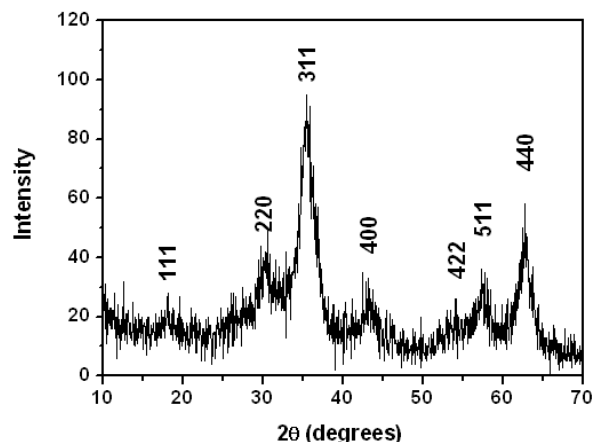


**Figure 2.** XRD pattern of the as-synthesized maghemite nanoparticles.

diffraction rings, which correspond to the (111), (311), (400), and (440) planes of the maghemite, respectively. This is in perfect agreement with the XRD results to be presented below (figure 2), indicating that the nanoparticles are well crystallized in spite of their ultrafine sizes.

The maghemite nanoparticles are subjected to further structural characterization with XRD and the result is shown in figure 2. Diffraction peaks at (111), (220), (311), (400), (440), and (511) are readily recognized from the XRD pattern. The observed diffraction peaks agree well with the tetragonal structure of maghemite (JCPDS file No 25-1402). It is clear that no other phases except the maghemite are detectable. This high purity of the as-synthesized maghemite nanoparticles is noteworthy given that side products such as Fe(OH)<sub>3</sub> or  $\alpha$ -Fe<sub>2</sub>O<sub>3</sub> (haematite) are usually formed from chemical co-precipitation or mechanochemical procedures. The use of the limited amount of water in the form of hydrate of the salt reagents and the consequent short milling time seem to account for the high purity of our maghemite nanoparticles. The broadening of the peaks indicates the small crystalline sizes of the nanoparticles, which is translated into an average core size of 2.7 nm using the Debye–Scherrer formula for spherical particles. This value is in good agreement with that estimated by TEM sampling of 100 nanoparticles described above (2.9 nm). The small deviation may come from the fact that the very small particles are hardly discernable in TEM images and thus may be omitted in the measurements. Maghemite has a spinel structure with  $P4_132$  space group ( $a = 8.35$  Å;  $c = 25.02$  Å). Schematically, maghemite can be described as fcc magnetite but without the Fe<sup>2+</sup> cations. In order to respect the cell electroneutrality, these Fe<sup>2+</sup> cations are replaced by Fe<sup>3+</sup> cations and vacancies. Consequently, the  $\gamma$ -Fe<sub>2</sub>O<sub>3</sub> structure is the same as that of Fe<sub>3</sub>O<sub>4</sub> except that it contains vacancies and has a smaller cell parameter (835 pm for  $\gamma$ -Fe<sub>2</sub>O<sub>3</sub> versus 839 pm for Fe<sub>3</sub>O<sub>4</sub>). Unfortunately, XRD alone is not capable of distinguishing  $\gamma$ -Fe<sub>2</sub>O<sub>3</sub> clearly from Fe<sub>3</sub>O<sub>4</sub>, especially when the nanoparticles are ultrafine and the diffraction peaks are broad [19].

In order to verify the Fe<sub>2</sub>O<sub>3</sub> stoichiometry of the as-synthesized nanoparticles, we rely on energy dispersive x-ray spectroscopy (EDXS) and x-ray photoelectron spectroscopy

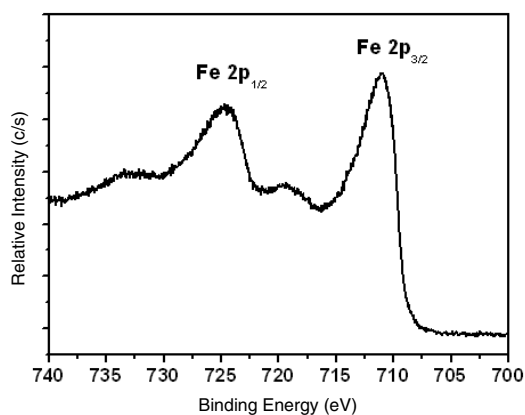


**Figure 3.** XPS spectrum (Fe 2p) of the as-synthesized maghemite nanoparticles.

(XPS). The EDXS spectrum is shown in the supporting information (figure S1) available at [stacks.iop.org/Nano/17/5812](https://stacks.iop.org/Nano/17/5812). Three peaks can be seen in the spectrum. The first at 530 eV is easily identified as the K edge of O, the second around 1739 eV corresponds to the K edge of Si, and the third around 7110 eV is assigned to the K edge of Fe. The trace amount of silicon (2.03 at.%) is believed to come from attrition of the porcelain mortar during milling of the reactant mixture. By peak integration, an estimation of the relative amounts of oxygen and iron is obtained. The calculated atomic ratio of O/Fe according to EDXS is 1.53, which is nearly the same as that of the theoretical value of iron (III) oxide (1.50). This consolidates the conclusion that our synthesized nanoparticles are iron (III) oxide.

The surface specificity of XPS makes it a useful analytical technique for the direct characterization of our ultrafine iron oxide nanoparticles [26–28]. Shown in figure 3 is the XPS spectrum of Fe(2p) for the as-prepared dried nanoparticle powder. The binding energy values for the main peak maxima  $2p_{3/2}$  and  $2p_{1/2}$  are found to be 710.9 and 724.7 eV, respectively. The values again are quite close to those reported for maghemite [27, 28]. Besides,  $dE = 13.6$  eV, the difference in the binding energies of the main peaks, is found to be higher than that reported for  $Fe_3O_4$  (13.21 eV) [27]. All these observations clearly indicate the absence of a component corresponding to octahedral  $Fe^{2+}$  in the present spectrum of Fe(2p). This further suggests the absence of impurities corresponding to  $Fe_3O_4$ .

The structural data presented above have revealed some favourable characteristics of our maghemite nanoparticles including the ultrafine particle size and narrow particle size distribution, and at the same time the good crystallinity and phase purity. These excellent properties make the maghemite MIONs a good candidate for the potential application as an MRI contrast agent. In order to investigate the magnetic properties of the as-synthesized nanoparticles, a VSM measurement was carried out. Illustrated in figure 4 is a magnetization curve of the maghemite nanoparticles measured at room temperature. The as-synthesized maghemite nanoparticles display a superparamagnetic behaviour, as evidenced by a zero coercivity and remanence on the magnetization loop. The sample could not be magnetically saturated at the magnetic

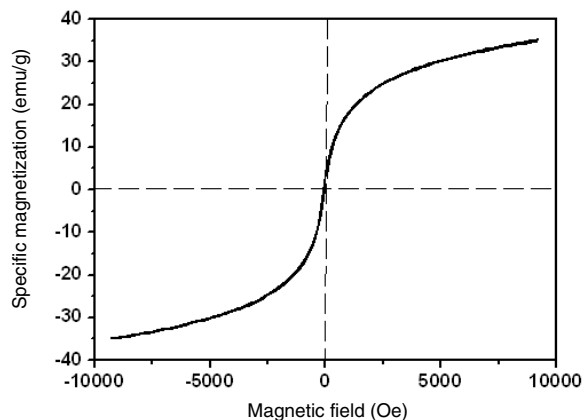


**Figure 4.** Magnetization curve of the as-synthesized maghemite nanoparticles at room temperature.

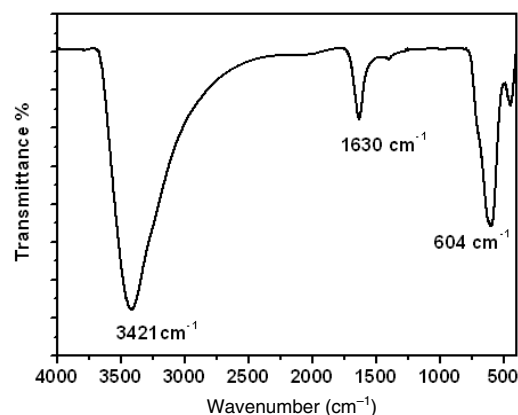


**Figure 5.** FTIR spectrum of the as-synthesized maghemite nanoparticles.

field limit of our VSM (1 T). The magnetization value obtained at 9000 Oe was  $34.7 \text{ emu g}^{-1}$ , which is quite close to those of the  $Fe_3O_4$  nanoparticles protected by  $(N(CH_3)_4OH)$  ( $40 \text{ emu g}^{-1}$ ) reported previously [3] and the MIONs used for MRI CAs by Weissleder *et al* [6]. However, it is much lower than the saturation magnetization of bulk maghemite ( $M_s = 76 \text{ emu g}^{-1}$  [29]), which could be explained by the small-particle surface effect and the internal cation disorder [30, 31].

Figure 5 shows an FTIR spectrum of the maghemite nanoparticles. Three major peaks are observed. The sharp peak around  $1630 \text{ cm}^{-1}$  and the broad peak from  $2400$  to  $3600 \text{ cm}^{-1}$  correspond, respectively, to the bending and stretching vibrations of the absorbed water molecules and the surface  $-OH$  groups [3, 32]. The weaker peak at  $448 \text{ cm}^{-1}$  and the moderately strong peak at  $604 \text{ cm}^{-1}$  are ascribed to the oxy- ( $Fe-O-Fe$ ) and hydroxyl ( $Fe-OH$ ) stretching vibrations [33]. These strong peaks indicate that the products are well crystallized. The FTIR spectrum indicates that the nanoparticles are rich in surface water and have abundant surface  $-OH$  groups. This result accounts in part for the excellent aqueous dispersion ability of our maghemite nanoparticles. Indeed, as will be shown below by thermal analysis, our maghemite nanoparticles, even after being dried, have a water content of as much as about 11%.

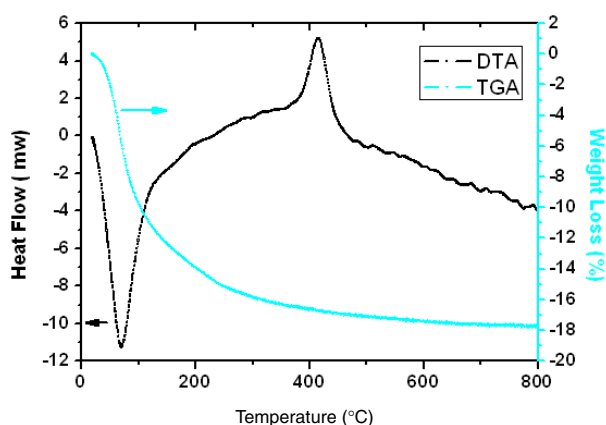


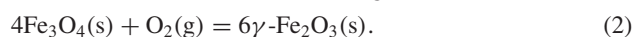
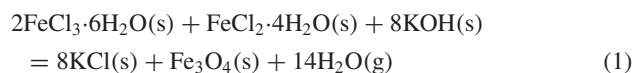
**Figure 6.** Thermogravimetric analysis profiles of the as-synthesized maghemite nanoparticles.

In order to attain further information on the surface groups (e.g.  $-\text{OH}$ ) and adsorbates (e.g.  $\text{H}_2\text{O}$ ) of the MIONs and study their thermal/chemical stability, DTA and TGA were carried out and the result is shown in figure 6. The strong and sharp endothermic peak around  $70^\circ\text{C}$  in the DTA curve can be assigned to the loss of the surface absorbed water, which corresponds to a weight loss of 11% in  $120^\circ\text{C}$  in the TGA curve. As the temperature is raised to  $800^\circ\text{C}$ , the total loss of weight reaches about 18%. Though there is no clear line between the loss of surface absorbed water and the loss of hydroxyl groups, a rough estimation gives a contribution of  $\sim 7\%$  weight loss from the hydroxyl group. Next, a sharp exothermic peak appears from  $360$  to  $440^\circ\text{C}$  in the DTA curve, which is associated with the  $\gamma$ -to- $\alpha$  phase transition. This is verified by the XRD pattern of a powder sample after heat treatment at  $450^\circ\text{C}$ ; the diffraction peaks are all ascribable to  $\alpha\text{-Fe}_2\text{O}_3$ , indicating the completeness of the phase transformation (see supporting information S2 available at [stacks.iop.org/Nano/17/5812](https://stacks.iop.org/Nano/17/5812)). This phase transition temperature  $T_{\gamma \rightarrow \alpha}$  is much lower than that of the corresponding microcrystalline particles ( $500\text{--}600^\circ\text{C}$ ), which is clearly due to the ultrafine size of our MIONs [34–37]. At the ultrafine scale, excess free energy allows the atoms or ions to diffuse more easily with a lower activation energy and therefore the thermal activated transformation occurs at a lower temperature than in the bulk counterpart [36].

Aqueous dispersity is essential to biological application for the MION nanoparticles. Significantly, our maghemite nanoparticles can be readily dispersed into concentrated aqueous colloid ( $>0.1\text{ M}$ ) as ferrofluid without addition of any surfactants, which is suitable for many medical applications, especially in MRI [3, 4, 6, 38, 39]. This remarkable aqueous dispersing ability can be better understood after a discussion on the salt-assisted solid-state reaction mechanism and resulting nanoparticle surface properties, which will be presented below.

Xin *et al* first reported salt-assisted solid-state reactions to synthesize nanocrystals of oxides ( $\text{CuO}$ ,  $\text{SnO}_2$ ), sulfides ( $\text{CuS}$ ,  $\text{ZnS}$ ,  $\text{CdS}$ ,  $\text{PbS}$ ), oxalates  $\text{M}_2(\text{C}_2\text{O}_4)_3 \cdot 3\text{H}_2\text{O}$  ( $\text{M} = \text{Nb}$ ,  $\text{La}$ ), and carbonates  $\text{MCO}_3$  ( $\text{M} = \text{Ca}$ ,  $\text{Ba}$ ) using hydrated metal salts as the starting materials. The solid-state metathesis reactions are highly exothermic and self-propagating and can proceed at ambient temperature in air to give nanocrystals with

a narrow size distribution [40, 41]. In our synthesis, multiple reagents in hydrated forms are employed. First,  $\text{FeCl}_2 \cdot 4\text{H}_2\text{O}$  and  $\text{FeCl}_3 \cdot 6\text{H}_2\text{O}$  react with  $\text{KOH}$  to give  $\text{Fe}_3\text{O}_4$  nanocrystals. Then under the reaction-generated heat and air oxidation, the ultrafine  $\text{Fe}_3\text{O}_4$  nanoparticles are converted to  $\gamma\text{-Fe}_2\text{O}_3$ . The reactions are shown in the following:



These reactions are plausible. In fact, Lin *et al* used anhydrous ferric and ferrous chlorides as reactants for the solid-state synthesis of magnetite nanoparticles under Ar atmosphere, which is essentially the first step of our reaction [21]. Moreover, in most cases maghemite nanoparticles were reportedly synthesized by direct air-oxidation of magnetite nanoparticles [42–44]. It is worth pointing out that when only  $\text{FeCl}_3 \cdot 6\text{H}_2\text{O}$  was used, we obtained a powder that can be attributed to a mixture of haematite and maghemite according to the XRD pattern (see supporting information S3 available at [stacks.iop.org/Nano/17/5812](https://stacks.iop.org/Nano/17/5812)). The diffraction peaks are quite weak and noisy, indicating that the nanoparticles are not well crystallized. From the TEM images of the powder (see supporting information S4 available at [stacks.iop.org/Nano/17/5812](https://stacks.iop.org/Nano/17/5812)), it was found that the nanoparticles are mostly less than 2 nm and their shapes quite irregular. Clearly, a combination of  $\text{FeCl}_2 \cdot 4\text{H}_2\text{O}$  and  $\text{FeCl}_3 \cdot 6\text{H}_2\text{O}$  reagents is needed to synthesize maghemite nanoparticles.

It is noticed that the use of hydrated reagents facilitates the formation of the maghemite nanoparticles; only 1 h of milling is required instead of many days with anhydrous reagents. One can imagine that the crystalline water is more weakly bound and thus could easily open the coordination sites of metal ions for attack, thus reducing the activation energy and increasing the reaction rates under our conditions. Simultaneously, as the maghemite nanoparticles are formed during the mechanochemical reaction,  $\text{KCl}$  and free water are produced as well and they are expected to give a saturated aqueous solution of  $\text{KCl}$ . The constant formation and precipitation of  $\text{KCl}$  from the  $\text{KCl}$  aqueous solution gives rise to  $\text{KCl}$  ‘shells’ surrounding the maghemite nanoparticles, preventing them from aggregating into larger particles. Under the reaction condition, the diffusion of solid particles of reactants is expected to be short-ranged, and this unique feature helps to yield a uniform and ultrafine size of the nanoproducts [40]. After the formation of the nanoparticles, the ‘shells’ of salt and surface water together with the dilution effect of the intervening salt matrix keep the nanoparticles isolated instead of agglomerating into large secondary and tertiary particles. Another consequence of the saturated-salt matrix in the solid-state synthesis is the dense coverage of hydroxyl groups on the nanoparticle surfaces. With the abundant hydroxyl groups on the nanoparticle surfaces, the maghemite nanoparticles could form a well dispersed aqueous colloid in high concentration ( $0.11\text{ M}$ ). The concentrated aqueous colloid was still stable after storing for 6 months due probably to electrostatic stabilization. As was reported previously [45–47], hydrous iron oxides have amphoteric character. The  $\text{Fe-OH}$  sites on the maghemite nanoparticle surface can react with  $\text{H}^+$  or  $\text{OH}^-$  ions from dissolved acids

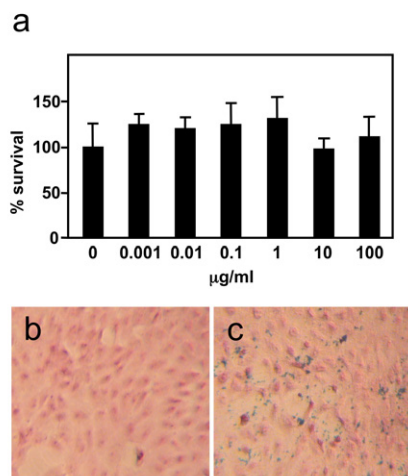
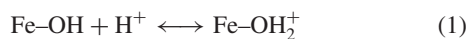
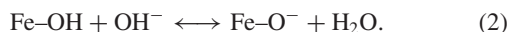


**Figure 7.** (a) WST-1 assay of the percentage survival of cells exposed to various concentrations of maghemite nanoparticles as compared to that of the non-exposure control cells. No obvious difference in the cell morphology was noticed under phase contrast inverted microscope between control cells (b) and the cells cultured in the presence of  $10 \text{ mg ml}^{-1}$  of nanoparticles (c). The blue colour in (c) was the results of Pearl's iron stain for the maghemite nanoparticles. The cells are counter-stained with Nuclear Fast Red.

or bases, leading to positive ( $\text{Fe-OH}_2^+$ ) or negative ( $\text{Fe-O}^-$ ) charges. In other words, the charges develop on the surface depending on the pH of the electrolyte solution:



or



In our salt-assisted solid-state reactions, KOH was used as one of the reactants, providing a basic condition. As a result, negative ( $\text{Fe-O}^-$ ) charges accumulate on the surfaces of the as-synthesized maghemite nanoparticles. An electrophoresis experiment has determined that the surfaces of the colloidal nanoparticles are negatively charged (see supporting information S5 at [stacks.iop.org/Nano/17/5812](https://stacks.iop.org/Nano/17/5812)). It is the electrostatic repulsion between the negatively charged nanoparticles that keeps the colloidal solution stable even at a high concentration. This colloidal solution could be kept stable for 6 months.

### 3.2. Cytotoxicity analysis

The *in vitro* biocompatibility of the nanoparticles was evaluated by WST-1 assay using Vero cells. As shown in figure 7(a), the survival of Vero cells was not inhibited by exposure to nanoparticles at all test concentrations ( $0\text{--}100 \text{ } \mu\text{g ml}^{-1}$ ). The cellular morphology was not significantly affected by the iron oxide nanoparticles, which were stained blue by Pearl's method (figure 7(c)) as compared to the control group in culture medium alone (figure 7(b)). As MIONs are usually used at concentrations as low as  $1 \text{ } \mu\text{g Fe/g}$  tissue to provide significant image contrast effect in clinical practice, our maghemite nanoparticles are considered to be biocompatible and could be further explored for advanced biomedical applications.

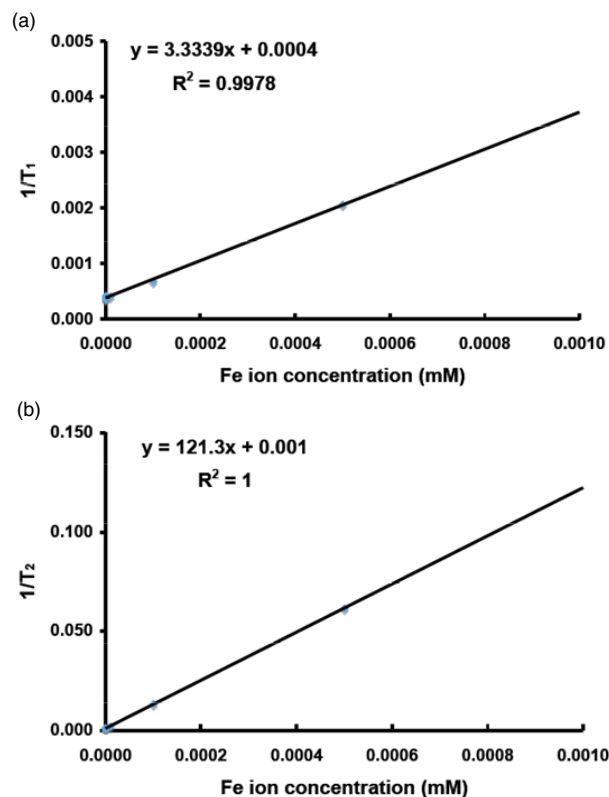


**Figure 8.** (a)  $r_1$  measurement of aqueous colloid of maghemite nanoparticles in the water by a 3 T clinical imager; (b)  $r_2$  measurement of aqueous colloid of maghemite nanoparticles in the water by a 3 T clinical imager.

### 3.3. Haemocompatibility test

The haemocompatibility is required for materials to be applied into circulation. In this experiment, the presence of haemoglobin from lysed red blood cells was measured and calculated as an index to reflect the haemocompatibility. From the haemocompatibility test results, our maghemite nanoparticles at all test concentrations (from 0.1 to 1000 nM iron concentration) showed haemocompatible results and thus could be further investigated for their *in vivo* bio-applications.

### 3.4. Relaxivity ( $r_1$ and $r_2$ ) measurements

Longitudinal and transversal relaxation times of the water protons ( $T_1$  and  $T_2$ ) have been measured for the aqueous dispersion of the maghemite nanoparticles synthesized in this work. The magnetic nanoparticles strongly reduce both relaxation times ( $T_1$  and  $T_2$ ) but with the  $T_2$  reduction significantly larger than the  $T_1$  reduction in pure water. At an iron concentration of 0.5 mM, the longitudinal relaxation time  $T_1$  was reduced from 2481 to 483 ms, while the  $T_2$  relaxation time was reduced from 996 ms to 16.23 ms. Both  $r_1$  and  $r_2$  relaxivities in  $\text{ms}^{-1} \text{ M}^{-1}$  were determined from least-square determination of the slopes of  $1/T_1$  and  $1/T_2$  versus molar concentrations of the nanoparticles from 0 to 1 mM (see figures 8(a) and (b)). The calculated  $r_1$  and  $r_2$  relaxivities of the maghemite nanoparticles are 3.334 and  $121.3 \text{ ms}^{-1} \text{ M}^{-1}$ , respectively. The superparamagnetic nanoparticles are called

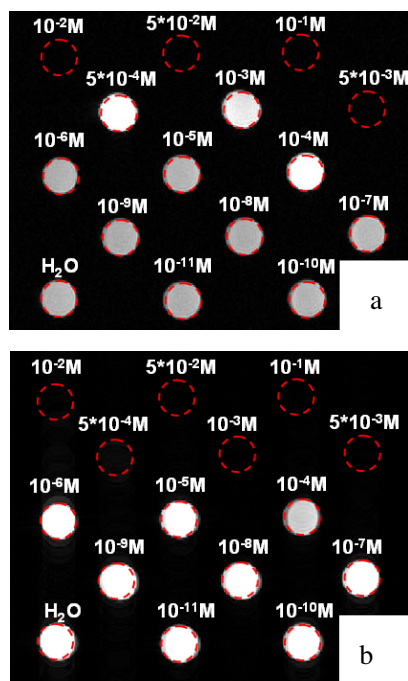


**Figure 9.**  $T_1$ -weighted (a) and  $T_2$ -weighted MRI images of the maghemite nanoparticles.

' $T_2$  agents' because they work mainly by reducing the  $T_2$  relaxation time.  $r_2$  values ranging from 10 to 500  $\text{ms}^{-1} \text{M}^{-1}$  Fe have been reportedly used for CAs based on iron oxide nanoparticles with different sizes, coatings and aggregation states [2–6, 39, 48]. Thus, our maghemite nanoparticles have favourable  $r_2$  relaxivity and can be applied as MRI CAs.

### 3.5. MRI measurement of the nanoparticle dispersions

The signal contrast enhancement performance of the as-synthesized nanoparticles was evaluated in a clinical MR imager and the results are given in figure 9. The images of pure water were also taken for reference.  $T_1$ -weighted MR images are presented in figure 9(a). It can be seen that when the Fe concentration is greater than  $10^{-5}$  M, the image of the ferrofluid is brighter than that of the pure water. Such a result indicates that our iron oxide nanoparticles could improve  $T_1$  enhancement, which is consistent with the other USPIOs used in MR angiography [49]. In the case of  $T_2$ -weighted MR images shown in figure 9(b), when the Fe concentration was greater than  $10^{-4}$  M, the image of the ferrofluid became darker than that of the pure water instead due to the  $T_2$  shortening. The *in vitro*  $T_2$  images suggest that the as-synthesized MION nanoparticles have potential application as negative contrast imaging agents. For example, tumours are often deficient in their ability to take up the magnetic materials and appear lighter against normal background tissue than they would without contrast agent.

As we know, superparamagnetic iron oxide nanoparticles have attracted decades of studies for MRI contrast agents [2–6]. Large particles, e.g. conventional polycrystalline iron oxide aggregates, are largely phagocytosed by cells of the reticuloendothelial system (liver, spleen, bone marrow, lung,

etc). These large particles are not capable of targeting other parts in the body, e.g. the pancreas, for which our MIONs may offer a solution. In general, large particles have the disadvantage of rapid immunologic recognition, which may elicit an immune response. Very small particles such as MION may pass fenestrated capillary endothelium, leave the space easily at sites of disrupted capillaries and reach the interstitium in large quantities. Once in the interstitium, very small particles are either specifically recognized by immunogenic sites (immunospecific imaging agents), receptors (receptor specific imaging agents), or active surface groups (lectin targeted imaging agents), or they are cleared by lymphatic fluid and eventually accumulate in lymph nodes. Until now, however, all the MIONs have been wrapped with dextran, starch or albumin for aqueous dispersion [13, 14, 49–53]. These polymer coatings significantly increase the particle size, which may affect their penetration and metabolic clearance rates in the body. The ultrafine, cap-free maghemite MION nanoparticles synthesized in this work can be very well dispersed into aqueous colloid for MRI contrast agent and this opens a new alternative to the dilemma.

## 4. Conclusions

To summarize, the maghemite MION nanoparticles with a mean diameter of 2.7 nm and a narrow particle size distribution ( $\sim 1$ –5 nm) have been synthesized by a salt-assisted solid-state reaction. The key is the use of multiple hydrated reagents and salt matrix, which facilitate the formation of the desired products. The nanoparticles are well crystallized and display good superparamagnetic properties. The abundant surface hydroxyl groups allow the nanoparticles to be dispersed into highly concentrated colloidal ferrofluids in water and also permit further biochemical functionalizations. WST-1 assay cytotoxicity analysis shows that the nanoparticles have good biocompatibility in clinical dosage. Relaxivity measurements show that the  $r_1$  and  $r_2$  relaxivities of the maghemite nanoparticles were 3.334 and 121.3  $\text{ms}^{-1} \text{M}^{-1}$ , respectively. With further surface modification by conjugating some bioactive molecules, macromolecules, to these nanoparticles, the obtained maghemite nanoparticles will find wide applications in targeted MRI imaging, cell labelling, hyperthermia, drug delivery, etc.

## Acknowledgments

This project is supported by the Industrial Technology Council (ITC069/02) and the National Science Council of Taiwan (NSC-94-2120-M-002-004 and NSC94-2314-B-006-067). SY wishes to thank the Hong Kong Young Scholar Cooperation Research Foundation of NSFC.

## References

- [1] Battle X and Labarta A 2002 *J. Phys. D: Appl. Phys.* **35** R15–42
- [2] Wang Y X J, Hussain S M and Krestin G P 2001 *Eur. Radiol.* **11** 2319–31
- [3] Cheng F Y, Su C H, Yang Y S, Yeh C S, Tsai C Y, Wu C L, Wu M T and Shieh D B 2005 *Biomaterials* **26** 729–38



- [4] Shieh D B, Cheng F Y, Su C H, Yeh C S, Wu M T, Wu Y N, Tsai C Y, Wu C L, Chen D H and Chou C H 2005 *Biomaterials* **26** 7183–91
- [5] Kim D K, Zhang Y, Kehr J, Klason T, Bjelke B and Muhammed M 2001 *J. Magn. Magn. Mater.* **225** 256–61
- [6] Weissleder R, Elizondo G, Wittenberg J, Rabito C A, Bengele H H and Josephson L 1990 *Radiology* **175** 489–93
- [7] Voltairas P A, Fotiadis D I and Michalis L K J 2002 *Biomechanics* **35** 813–21
- [8] Jordan A, Scholz R, Wust P, Fahling H, Krause J, Wlodarczyk W, Sander B, Vogl T and Felix R 1997 *Int. J. Hyperth.* **13** 587–605
- [9] Shinkai M, Yanase M, Suzuki M, Honda H, Wakabayashi T, Yoshida J and Kobayashi T 1999 *J. Magn. Magn. Mater.* **194** 176–84
- [10] Jordan A, Scholz R, Wust P, Fahling H and Felix R 1999 *J. Magn. Magn. Mater.* **201** 413–9
- [11] Mornet S, Vasseur S, Grasset F and Duguet E 2004 *J. Mater. Chem.* **14** 2161–75
- [12] Bonnemain B 1998 *J. Drug Target.* **6** 167–74
- [13] Weissleder R, Lee A S, Khaw B A, Shen T and Brady T J 1992 *Radiology* **182** 381–5
- [14] Weissleder R, Lee A S, Fischman A J, Reimer P, Shen T, Wilkinson R, Callahan R J and Brady T J 1991 *Radiology* **181** 245–9
- [15] Jiang W, Yang H C, Yang S Y, Horng H E, Hung J C, Chen Y C and Hong C Y 2004 *J. Magn. Magn. Mater.* **283** 210–4
- [16] Feltin N and Pileni M P 1997 *Langmuir* **13** 3927–33
- [17] Kang Y S, Risbud S, Tabolt J P and Stroeve P 1996 *Chem. Mater.* **8** 2209–12
- [18] Hyeon T, Lee S S, Park J, Chung Y and Na H B 2001 *J. Am. Chem. Soc.* **123** 12798–801
- [19] Janot R and Guerard D 2002 *J. Alloys Compounds* **333** 302–7
- [20] Randrianantoandro N, Mercier A M, Hervieu M and Greneche J M 2001 *Mater. Lett.* **47** 150–8
- [21] Lin C R, Chu Y M and Wang S C 2006 *Mater. Lett.* **60** 447–50
- [22] Choi H, Choi S R, Zhou R, Kung H F and Chen I W 2004 *Acad. Radiol.* **11** 996–1004
- [23] Morales M P, Miguel O B, Alejo R P, Cabello J R, Verdaguer S V and Grady K O 2003 *J. Magn. Magn. Mater.* **266** 102–9
- [24] Bellin M F, Beigelman C and Precetti-Morel S 2000 *Eur. J. Radiol.* **34** 257–64
- [25] Thode K, Luck M, Schroder W, Semmler W, Blunk T, Muller R H and Kresse M 1997 *J. Drug Target.* **5** 35–43
- [26] Harvey D T and Linton R W 1981 *Anal. Chem.* **53** 1684–8
- [27] Banerjee I, Kholam Y B, Balasubramanian C, Pasricha R, Bakare P P, Patil K R, Das A K and Bhoraskar S V 2006 *Scr. Mater.* **54** 1235–40
- [28] Fujii T, de Groot F M F, Sawatzky G A, Voogt F C, Hibma T and Okada K 1999 *Phys. Rev. B* **59** 3195–202
- [29] Montagne F, Mondain-Monval O, Pichot C, Mozzanega H and Elaissari A 2002 *J. Magn. Magn. Mater.* **250** 302–12
- [30] Martinez B, Obradors X, Balcells L, Rouanet A and Monty C 1998 *Phys. Rev. Lett.* **80** 181–4
- [31] Yu S and Chow G M 2004 *J. Mater. Chem.* **14** 2781–6
- [32] Sibin C P, Kumar S R, Mukundan P and Warriar K G K 2002 *Chem. Mater.* **14** 2876–81
- [33] Khaleel A A 2004 *Chem. Eur. J.* **10** 925–32
- [34] Chhabra V, Ayyub P, Chatopadhyay S and Maitra A N 1996 *Mater. Lett.* **26** 21–6
- [35] Morales M P, Pecharroman C, Carreñ T G and Serna C J 1994 *J. Solid State Chem.* **108** 158–63
- [36] Ennas G, Marongiu G and Musinu A 1999 *J. Mater. Res.* **14** 1570–5
- [37] Torres Sanchez R M 1996 *J. Mater. Sci. Lett.* **15** 461–2
- [38] Sous M H, Rubim J C, Sobrinho P G and Tourinho F A 2001 *J. Magn. Magn. Mater.* **225** 67–72
- [39] Babes L, Denizot B, Tanguy G, Jeune J J L and Jallet P 1999 *J. Colloid Interface Sci.* **212** 474–82
- [40] Ye X R, Jia D Z, Yu J Q, Xin X Q and Xue Z L 1999 *Adv. Mater.* **11** 941–2
- [41] Li F, Xu J Q, Yu X H, Chen L Y, Zhu J M, Yang Z R and Xin X Q 2002 *Sensors Actuators B* **81** 165–9
- [42] Sun Y K, Ma M, Zhang Y and Gu N 2004 *Colloids Surf. A* **245** 15–9
- [43] Lee S J, Jeong J R, Shin S C, Kim J C and Kim J D 2004 *J. Magn. Magn. Mater.* **282** 147–50
- [44] Kang Y S, Risbud S, Rabolt J F and Stroeve P 1996 *Chem. Mater.* **8** 2209–11
- [45] Liu Z L, Liu Y J, Yao K L, Ding Z H, Tao J and Wang X 2002 *J. Mater. Synth. Process.* **10** 83–7
- [46] Illés E and Tombácz E 2006 *J. Colloid Interface Sci.* **295** 115–23
- [47] Sun Z X, Su F W, Forsling W and Samskog P O 1998 *J. Colloid Interface Sci.* **197** 151–9
- [48] Coroiu I 1999 *J. Magn. Magn. Mater.* **201** 449–52
- [49] Wagenseil J E, Johansson L O M and Lorenz C H 1999 *J. Magn. Reson. Imaging* **10** 784–9
- [50] Weissleder R 1996 *US Patent Specification* 5492814
- [51] Hogemann D, Josephson L, Weissleder R and Basilion J P 2000 *Bioconjug. Chem.* **11** 941–6
- [52] Zhang Y, Kohler N and Zhang M 2002 *Biomaterials* **23** 1553–61
- [53] Gamarra L F, Brito G E S, Pontuschka W M, Amaro E, Parma A H C and Goya G F 2005 *J. Magn. Magn. Mater.* **289** 439–41